

Microsecond dynamics in proteins by two-dimensional ESR. II. Addressing computational challenges

Cite as: J. Chem. Phys. **154**, 084115 (2021); <https://doi.org/10.1063/5.0042441>

Submitted: 30 December 2020 . Accepted: 29 January 2021 . Published Online: 24 February 2021

 Pranav Gupta,  Kevin Chaudhari, and  Jack H. Freed



View Online



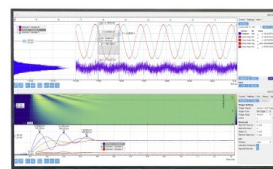
Export Citation



CrossMark

Challenge us.

What are your needs for
periodic signal detection?



Zurich
Instruments

Microsecond dynamics in proteins by two-dimensional ESR. II. Addressing computational challenges

Cite as: J. Chem. Phys. 154, 084115 (2021); doi: 10.1063/5.0042441

Submitted: 30 December 2020 • Accepted: 29 January 2021 •

Published Online: 24 February 2021



View Online



Export Citation



CrossMark

Pranav Gupta,¹  Kevin Chaudhari,²  and Jack H. Freed^{1,a)} 

AFFILIATIONS

¹National Biomedical Center for Advanced ESR Technology and Department of Chemistry and Chemical Biology, Cornell University, Ithaca, New York 14853, USA

²Department of Computer Science, Cornell University, Ithaca, New York 14853, USA

^{a)} Author to whom correspondence should be addressed: jhf3@cornell.edu

ABSTRACT

Two-dimensional electron–electron double resonance (2D-ELDOR) provides extensive insight into molecular motions. Recent developments permitting experiments at higher frequencies (95 GHz) provide molecular orientational resolution, enabling a clearer description of the nature of the motions. In previous work, we provided simulations for the case of domain motions within proteins that are themselves slowly tumbling in a solution. In order to perform these simulations, it was found that the standard approach of solving the relevant stochastic Liouville equation using the efficient Lanczos algorithm for this case breaks down, so algorithms were employed that rely on the Arnoldi iteration. While they lead to accurate simulations, they are very time-consuming. In this work, we focus on a variant known as the rational Arnoldi algorithm. We show that this can achieve a significant reduction in computation time. The stochastic Liouville matrix, which is of very large dimension, N , is first reduced to a much smaller dimension, m , e.g., from $N \sim O(10^4)$ to $m \sim 60$, that spans the relevant Krylov subspace from which the spectrum is predicted. This requires the selection of the m frequency shifts to be utilized. A method of adaptive shift choice is introduced to optimize this selection. We also find that these procedures help in optimizing the pruning procedure that greatly reduces the dimension of the initial N dimensional stochastic Liouville matrix in such subsequent computations.

Published under license by AIP Publishing. <https://doi.org/10.1063/5.0042441>

I. INTRODUCTION

Slow motional pulsed ESR spectroscopy methods such as 2D-ELDOR help to unravel complex motional dynamics such as in polymers, liquid crystals, membranes, and proteins.^{1–7} Technological developments in high-power pulsed ESR now enable such studies to be performed at higher frequency (95 GHz) wherein real time observation from nanoseconds to microseconds may be realized with good orientational resolution.^{8–15} Analyzing these experimental spectra requires the use of tracking the time evolution of the orientation dependent electron spin density matrix in Liouville space via the stochastic Liouville equation (SLE). The stochastic Liouville matrices corresponding to slow motions and high frequency are highly non-normal, sparse, and large-scale, thus necessitating

the use of efficient Krylov subspace methods.^{16–24} These methods have enjoyed success in the magnetic resonance community for several decades, where the Lanczos algorithm has been successfully employed. But we face an important challenge in making these calculations fast and accurate for very slow motions, especially when dealing with multiple spin labels, ordering potentials, and the need to perform hundreds of independent computations during non-linear least squares fits to experimental data. While simulating ESR spectra with multiple pulse sequences, especially at high frequencies (~ 95 GHz) and slow motions $R \lesssim 10^7$ s⁻¹, one needs to evaluate resolvents and/or matrix exponentials at hundreds of frequency/time points^{17,25} when Lanczos methods break down. Current methods do not exploit the fact that these various resolvents and matrix exponentials actually come from the same Krylov

subspace. However, to span this entire Krylov subspace efficiently, we need specialized techniques that adaptively scan the entire Krylov subspace with minimal matrix vector multiplications and sufficient accuracy. Therefore, in this work, we introduce rational Krylov methods that demonstrate a substantial increase in speed and a similar decrease in requirements for storing resolvent vectors in the case of 2D-ELDOR as compared to our previous work.²⁵ We describe the main concepts behind rational Krylov methods and analyze in detail the time advantages for the example of 2D-ELDOR. We briefly discuss possibilities for further improvements.

II. KRYLOV SUBSPACE TECHNIQUES IN ESR: AN OVERVIEW

A. Stochastic Liouville equation

The analysis of ESR experiments requires us to consider both the rotational and the spin degrees of freedom of the electron spin probe under consideration. The Stochastic Liouville Equation (SLE)^{17,26,27} is an accurate representation of this dynamics,

$$\begin{aligned} \frac{\partial \rho(\Omega, t)}{\partial t} &= (-i\mathcal{H}^\times - \Gamma(\Omega))(\rho(\Omega, t) - \rho_{eq}(\Omega)) \\ &:= -\mathcal{L}(\rho(\Omega, t) - \rho_{eq}(\Omega)). \end{aligned} \quad (1)$$

Here, ρ is the time (t)- and orientation (Ω)-dependent electron spin density matrix with an equilibrium value $\rho_{eq}(\Omega)$ and \mathcal{H}^\times is the electron spin Hamiltonian superoperator ($\mathcal{H}^\times \rho$ is defined as $[\mathcal{H}, \rho]$). Γ is the classical, orientation-dependent relaxation superoperator of which rotational diffusion is the major component and \mathcal{L} is known as the *Liouville superoperator*. As suggested by the equation above, \mathcal{L} describes the combined effects of the electron spin Hamiltonian and the relaxation superoperator Γ .

The main task in computing CW/pulsed ESR spectra is to track the orientation-dependent density matrix under the effect of the Liouville superoperator, \mathcal{L} . Moreover, in the absence of a microwave field, \mathcal{L} is time-independent and maintains its coherence order p^S . This allows us to rewrite Eq. (1) in the following form:²⁷

$$\frac{\partial \rho(\Omega, t)}{\partial t} = -\mathcal{L}_{(p^S)}(\rho(\Omega, t) - \rho_{eq}(\Omega)). \quad (2)$$

Equivalently,

$$\rho(\Omega, t) - \rho_{eq}(\Omega) = e^{-\mathcal{L}_{(p^S)} t}(\rho(\Omega, 0) - \rho_{eq}(\Omega)). \quad (3)$$

In Liouville space, one represents ρ as a vector instead of a matrix, thus allowing us to represent \mathcal{L}_{p^S} as a linear transformation on the entries of ρ stretched out in a column format. The matrix representation of \mathcal{L}_{p^S} , under appropriate symmetry transformations, becomes complex symmetric.²⁷ For CW spectra, the free induction decay signal can be written as

$$I(t) \propto \langle v_0 | e^{-\mathcal{L}_{+1} t} | v_0 \rangle. \quad (4)$$

However, we are usually interested in the Fourier transform CW spectrum $I(f)$,²⁶

$$I(f) \propto \langle v_0 | (\mathcal{L}_{+1} - 2\pi i f \mathbb{I})^{-1} | v_0 \rangle. \quad (5)$$

Here, \mathcal{L}_{+1} denotes the stochastic Liouville matrix in the $p^S = +1$ coherence order, whereas \mathbb{I} denotes the identity matrix of the same dimensions as \mathcal{L}_{+1} .

In a two-dimensional ESR experiment such as 2D-ELDOR, we employ high-power microwave pulses in order to excite the widest possible bandwidth and yet these pulses are typically much shorter than the relaxation time scales of the electron spins. In these experiments, it is true that the electron spin coherence order, p^S , does not change between successive microwave pulses.²⁷ This simplifies the computation of the 2D-ELDOR spectrum and allows us to treat only the microwave pulse as leading to changes in the coherence order so that between successive pulses when the microwave field is absent, we just need to consider the effects of \mathcal{L} within the same coherence order. In other words, \mathcal{L} is block-diagonal with respect to p^S in its matrix representation.

Many coherence pathways, characterized by the values p^S , can occur between successive pulses. The unwanted pathways are filtered out by means of phase cycling, leaving the net signal measured in a 2D-ELDOR experiment. The motional dynamics is adequately captured by the remaining two coherence pathways, namely, S_{c+} and S_{c-} .^{1,13,27,28} Taken together, they form the hypercomplex 2D-ELDOR signal. However, the S_{c-} pathway is echo-like, whereas the S_{c+} is FID-like (cf. Fig. 1). As a result, the S_{c+} signal decays faster under the effects of the inhomogeneous broadening canceled out in the S_{c-} signal. For very slow-motions considered in this work, the S_{c+} signal emerging after the spectrometer dead-time is greatly reduced compared to the S_{c-} signal. Therefore, in this paper, we focus on the S_{c-} coherence pathway.

The 2D-ELDOR S_{c-} coherence pathway proceeds as follows: initially, the electron spins are in the longitudinal coherence ($p^S = 0$). The first $\frac{\pi}{2}$ pulse takes them to the coherence order $p^S = +1$. For a time t_1 , they remain in $p^S = +1$, then a $\frac{\pi}{2}$ pulse transforms them to $p^S = 0$ where they are “stored” along the negative z-axis. They remain for time T_{mix} in $p^S = 0$ after which they are transformed to $p^S = -1$ by the final $\frac{\pi}{2}$ pulse. Signal collection can be performed after the final $\frac{\pi}{2}$ pulse.

Hence, the S_{c-} signal is a function of t_1 , T_{mix} , and t_2 . However, 2D-ELDOR signals are generally represented by the frequency variables f_1 and f_2 , where f_1 and f_2 are Fourier conjugates to the time variables t_1 and t_2 , respectively. Mathematically,

$$S_{c-}(f_1, T_{mix}, f_2) = \iint S_{c-}(t_1, T_{mix}, t_2) e^{2\pi i f_1 t_1} e^{-2\pi i f_2 t_2} dt_1 dt_2. \quad (6)$$

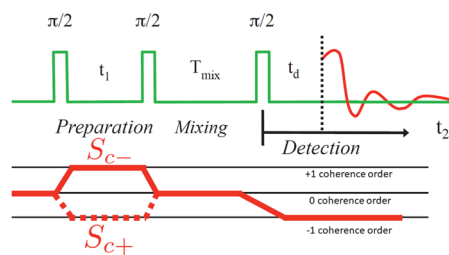


FIG. 1. A schematic of the 2D-ELDOR experiment with 3 $\frac{\pi}{2}$ -rotation microwave pulses. The coherence pathways S_{c+} and S_{c-} are also shown.

T_{mix} is fixed for a given 2D-ELDOR experiment. Note the receiver (or spectrometer) dead time t_d shown in the schematic. The 2D-ELDOR signal in the time interval t_d just after the final pulse is experimentally inaccessible.¹³ Current state-of-the-art 2D-ELDOR experiments at 95 GHz ESR frequency have $t_d \sim 20$ ns.^{13,14}

After Fourier transforming the times t_1 and t_2 into frequencies f_1 and f_2 , one may write as follows:²⁵

$$S_{c-}(f_1, T_{mix}, f_2) \propto \langle v_0 | (\mathcal{L}_{-1} + 2\pi i f_2 \mathbb{I})^{-1} \times P_{-1 \leftarrow 0} e^{-\mathcal{L}_0 T_{mix}} P_{0 \leftarrow -1} (\mathcal{L}_{+1} - 2\pi i f_1)^{-1} | v_0 \rangle. \quad (7)$$

Here, $|v_0\rangle := (\rho(\Omega, t = 0^+) - \rho_{eq}(\Omega))$ denotes the initial density matrix in the $p^S = +1$ coherence right after the first $\frac{\pi}{2}$ microwave pulse, $P_{a \leftarrow b}$ is the constant linear transformation matrix from $p^S = b$ to $p^S = a$ denoting the effect of the $\frac{\pi}{2}$ pulse, and $|\rangle, \langle|$ denote the usual bra-ket notation for a vector and its conjugate transpose.

B. Current Krylov subspace techniques

Notice the presence of resolvents of the form $(A - 2\pi i f \mathbb{I})^{-1}$ and matrix exponentials of the form e^{-At} in Eqs. (5) and (7). Any pulsed/CW ESR calculation has both or either of these matrix functions. As the $N \times N$ SLE matrices for slow motions and high frequencies might reach sizes as large as $100\,000 \times 100\,000$, with only $\sim 0.5\%$ of the elements being non-zero, direct methods such as LU factorization²⁹ become expensive in terms of time and memory. Also, matrix functions such as e^{-At} usually do not preserve sparsity. Therefore, for the past decades,^{16,21,23,30} the approach has been used to calculate expressions of SLE matrices such as $(A - 2\pi i f \mathbb{I})^{-1}v$ and $e^{-At}v$ by building up an iterative Krylov subspace of the matrix A and the vector v . The complex symmetric Lanczos algorithm,¹⁶ its complex symmetric conjugate gradient counterpart,^{17,31} and Arnoldi algorithms such as GMRES²⁵ have had significant success in terms of predicting cw and pulsed 2D-ELDOR ESR spectra. A typical algorithm computes resolvents or matrix exponentials for each frequency value f or a time point t with Algorithm 1 in the following way:

The function *Solve* is the iterative solver, viz., GMRES and BICGSTAB.

To calculate the 2D-ELDOR spectrum, we evaluate²⁵ $S_{c-}(f_i, f_j) \propto \langle z(f_j) | e^{-\mathcal{L}_0 T_{mix}} | z(f_i) \rangle$, where $f_i, f_j \in \{f_1, f_2, \dots, f_n\}$, by evaluating the action of the matrix exponential $e^{-\mathcal{L}_0 T_{mix}}$ on each of $z(f_i) = z(f_1), z(f_2), \dots, z(f_n)$ followed by an inner product with $z(f_j)$ according to Algorithm 2. Here, \mathcal{L}_0 denotes the stochastic Liouville operator in the $p^S = 0$ coherence order.

Typically, high frequency slow motional spectra are broad and span several hundred MHz, which means we need ~ 200 grid points to accurately simulate cw spectra and 250 grid points for 2D-ELDOR in each frequency variable, viz., f_1, f_2 , etc. (See the [supplementary material](#) section for a detailed explanation.) This means that we may

ALGORITHM 1. Pseudocode for calculating the CW spectrum.

Result: a set of n vectors $|z(f_i)\rangle$
for i in $\{1, 2, \dots, n\}$ **do**
 $|z(f_i)\rangle \leftarrow \text{Solve}((\mathcal{L}_{+1} - 2\pi i f_i \mathbb{I})x = v)$

ALGORITHM 2. Pseudocode for calculating the 2D-ELDOR spectrum.

Result: an $n \times n$ grid of spectrum values
for i in $\{1, 2, \dots, n\}$ **do**
 $|z(f_i)\rangle = \text{Solve}((A - 2\pi i f_i \mathbb{I})x = v)$
 $|y(f_i)\rangle = P_{0 \leftarrow +1} |z(f_i)\rangle$
 $|x(f_i)\rangle = e^{-\mathcal{L}_0 T_{mix}} |y(f_i)\rangle \leftarrow$ matrix exponential
for i in $\{1, 2, \dots, n\}$ **do**
for j in $\{1, 2, \dots, n\}$ **do**
 $S_{c-}(f_i, f_j) = \langle y(f_j) | x(f_i) \rangle$

need to evaluate the action of $e^{-\mathcal{L}_0 T_{mix}}$ on around 250 different vectors $z(f_i)$. The non-normality of \mathcal{L}_0 , combined with its extremely large dimension, makes this computation a significant bottleneck in the computation of 2D-ELDOR spectra at slow motions and high frequencies. In addition, a Krylov subspace technique might need to split T_{mix} into as many as 50 time steps in order to achieve sufficient accuracy.

This motivates us to ask the following question: is there a way to save on the number of calls to resolvent routines so that we save on the time required to compute several hundred resolvents and hence also save time further downstream when time-consuming matrix exponentials such as $e^{-\mathcal{L}_0 T_{mix}}$ have to act on multiple vectors $|z(f)\rangle$? While there are ~ 250 vectors in the set $\{z(f_1), z(f_2), \dots, z(f_n)\}$, i.e., $n \sim 250$, we shall show that we need many fewer to compute accurate pulsed ESR spectra. Before we discuss the new algorithm, we show this in a simple manner.

C. Number of effective dimensions in the Krylov subspace $\mathcal{K}(\mathcal{L}_{+1}, v_0)$

What we are claiming is that the Krylov subspace generated by \mathcal{L}_{+1} and the starting vector $|v_0\rangle$ has a dimension much less than the number of vectors in the set $\{z(f_1), z(f_2), \dots, z(f_n)\}$. To demonstrate this, we perform a singular value decomposition (SVD) of the $N_{+1} \times n$ matrix Z_{+1} formed by concatenating $\{z(f_1), z(f_2), \dots, z(f_n)\}$, where $|z(f_i)\rangle = (\mathcal{L}_{+1} - 2\pi i f_i \mathbb{I})^{-1} |v_0\rangle$ and N_{+1} is the dimension of \mathcal{L}_{+1} . The singular values of Z_{+1} for a nitroxide spin label ($I = 1$) with

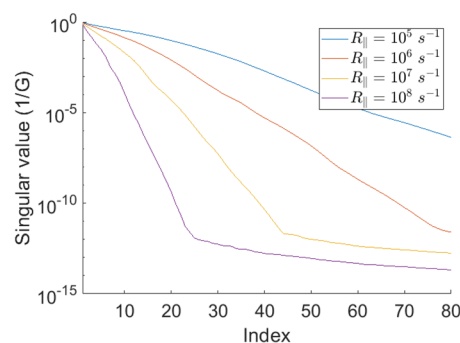


FIG. 2. Singular values of Z_{+1} for a nitroxide spin label. The singular values have units 1/G because \mathcal{L}_{+1} has units Gauss. The dimensions of \mathcal{L}_{+1} , i.e., N_{+1} , for $R_{||} = 10^8 \text{ s}^{-1}, 10^7 \text{ s}^{-1}, 10^6 \text{ s}^{-1}, 10^5 \text{ s}^{-1}$ are, respectively, 2582, 4700, 8951, and 17 249.

principal g tensor values $g_{xx} = 2.0087$, $g_{yy} = 2.0057$, $g_{zz} = 2.0021$ and principal A (hyperfine) tensor values $A_{xx} = 6$ G, $A_{yy} = 6$ G, $A_{zz} = 36$ G for various motional rates R_{\parallel} are shown in Fig. 2. The diffusion tilt angle $\beta_d = 90^\circ$. For simplicity, R_{\perp} is set to $0.5R_{\parallel}$. The ESR frequency is 95 GHz.

We see from Fig. 2 that only a relatively small number of singular values compared to N_{+1} are significant, and as the motions become faster, this number becomes smaller as expected. Thus, one might expect that a small subset of $\{z(f_i)\}$ would be sufficient to span the relevant Krylov subspace, i.e., Z_{+1} is expected to have a lower rank than N_{+1} consistent with the number of significant singular values.

III. IMPROVEMENT BY RATIONAL KRYLOV SUBSPACE METHODS

A. Motivation and overview of rational Krylov methods

We now seek a method that enables us to compute only the required basis vectors that span $\{z(f_1), z(f_2), \dots, z(f_n)\}$. The goal is to choose an adaptive set³² of m frequencies that can result in an accurate computation of $z(f) = (A - 2\pi f\mathbb{I})^{-1}|v_0\rangle$ for all of these n frequencies such that $m \ll n$.

Usual polynomial Krylov methods used in ESR, when run up to n iterations, typically span the space of all polynomial functions of the matrix $A - 2\pi f\mathbb{I}$ acting on the starting vector $|v_0\rangle$, i.e., $\{p(A)|v_0\} | \deg(p) \leq n\}$. Each time, we calculate $z(f_j) = (A - 2\pi f_j\mathbb{I})^{-1}|v_0\rangle$ for a given f_j , these n iterations build a fresh Krylov subspace to compute $z(f_j)$. However, all these individual Krylov subspaces for the different j are the same because for any value of f , we have

$$(A - 2\pi f\mathbb{I})^{-1}|v_0\rangle = (a_0(f) + a_1(f)A + a_2(f)A^2 + \dots)|v_0\rangle \quad (8)$$

for some sequence of coefficients $a_0(f), a_1(f), \dots$, that depends on f . In general, any function $g(A)|v_0\rangle$, irrespective of what g is, comes from the same Krylov subspace $\mathcal{K}(A, v_0)$.

While seeding the solution $z(f_{j-1})$ from a previous Krylov subspace iteration is a viable option,¹⁷ we have observed that it does not lead to substantial improvement in the overall time taken to compute $z(f_j)$ for the many values of f_j . That is, as noted earlier, one needs ~ 200 values of f_j for high frequency cw ESR spectra and ~ 250 for 2D-ELDOR in order to recover the detailed features regarding the motional dynamics that could be missed because of poorer frequency resolution.

We now wish to point out that rational Krylov methods will in a few iterations span a general³³ space of rational functions $p(A)/q(A)$ up to a certain order in A . The paradigm shift in rational Krylov methods comes from the fact that we gain significantly by replacing the standard matrix multiplications $A|v_0\rangle, A^2|v_0\rangle, \dots$, in our usual, polynomial Krylov subspace methods with $(A - \xi_1\mathbb{I})^{-1}A|v_0\rangle, (A - \xi_2\mathbb{I})^{-1}A|v_0\rangle, \dots$. The matrix inverses at each step help us span a more general Krylov subspace with much fewer basis vectors.³³ Having much fewer basis vectors helps us greatly, for example, in computing later stages of the pulse ESR sequences, where we have matrix exponentials such as $e^{-L_0 T_{mix}}$. Having to act only on a few, adaptively

chosen Krylov basis vectors rather than many vectors $z(f_i)$ will result in much faster computations.

While the literature on rational Krylov methods is vast, we focus on the rational Arnoldi algorithm^{32,34} as it suffices for our task. The following pseudocode, Algorithm 3, describes the rational Arnoldi algorithm,³⁵ which is akin to GMRES:

Let us consider this algorithm in more detail. In the first step, we calculate the non-orthogonalized rational Arnoldi vector,

$$\tilde{v}_{k+1} = (\mathbb{I} - A/\xi_k)^{-1}Av_k = -\xi_k(A - \xi_k\mathbb{I})^{-1}Av_k. \quad (9)$$

Notice the presence of ξ_k in Eq. (9). When all the ξ_k 's are chosen to be ∞ , Eq. (9) reduces to the regular Arnoldi iteration.

By orthogonalizing \tilde{v}_{k+1} with respect to v_1, v_2, \dots, v_k , we can write the following:

$$\tilde{v}_{k+1} = \sum_{i=1}^{k+1} h_{i,k}v_i. \quad (10)$$

Equation (10) holds for both rational and regular Arnoldi iterations.³² By combining Eqs. (9) and (10), we get

$$\begin{aligned} (\mathbb{I} - A/\xi_k)^{-1}Av_k &= \sum_{i=1}^{k+1} h_{i,k}v_i \\ \implies Av_k &= (\mathbb{I} - A/\xi_k)\sum_{i=1}^{k+1} h_{i,k}v_i \\ &= \sum_{i=1}^{k+1} h_{i,k}v_i - \xi_k^{-1}A\sum_{i=1}^{k+1} h_{i,k}v_i \\ \implies A\left(v_k + \xi_k^{-1}\sum_{i=1}^{k+1} h_{i,k}v_i\right) &= \sum_{i=1}^{k+1} h_{i,k}v_i. \end{aligned} \quad (11)$$

Define the unitary matrix constructed from the orthonormal vectors v_i , i.e., $V_m = [v_1, v_2, \dots, v_m]$ and $H_m(i, j) = h_{i,j}$, where $i, j \in \{1, 2, \dots, m\}$. Note that V_m is unitary under the Hermitian inner product $\langle x, y \rangle = x^\dagger y$. Now, let e_m be the m th basis vector and $D_m \equiv \text{diag}[\xi_1^{-1}, \xi_2^{-1}, \dots, \xi_m^{-1}]$ so that we can rewrite Eq. (11) as follows:

$$\begin{aligned} AV_m + AV_m H_m D_m + Av_{m+1} h_{m+1,m} \xi_m^{-1} e_m^T \\ = V_m H_m + v_{m+1} h_{m+1,m} e_m^T. \end{aligned} \quad (12)$$

Equation (12) can be rewritten as

$$AV_m K_m + Av_{m+1} h_{m+1,m} \xi_m^{-1} e_m^T = V_m H_m + v_{m+1} h_{m+1,m} e_m^T. \quad (13)$$

Here, $K_m = \mathbb{I}_m + H_m D_m$. Close to convergence, $h_{m+1,m}$ must reach negligible values, so we can write

$$AV_m K_m \approx V_m H_m. \quad (14)$$

ALGORITHM 3. Compute a rational Arnoldi basis for matrix A and starting vector $|v_0\rangle$.

Given: matrix A , starting vector $|v_0\rangle$, shifts $\{\xi_1, \xi_2, \dots\}$
Result: a set of $m + 1$ orthogonal rational Arnoldi vectors
 $\{v_k, k \in \{1, 2, 3, \dots, m + 1\}\}$

$\tilde{v}_1 = |v_0\rangle$, normalize $v_1 = |v_0\rangle / \|v_0\|$

for k in $\{1, 2, \dots, m\}$ **do**

$\tilde{v}_{k+1} = (\mathbb{I} - A/\xi_k)^{-1}Av_k$

for i in $\{1, 2, \dots, k\}$ **do**

$\perp \tilde{v}_{k+1} = \tilde{v}_{k+1} - (v_i^\dagger \tilde{v}_{k+1})v_i \leftarrow$ Gram-Schmidt orthogonalization

 Normalize $v_{k+1} = \tilde{v}_{k+1} / \|\tilde{v}_{k+1}\|$.

Or equivalently,

$$V_m^\dagger A V_m \approx H_m K_m^{-1}. \quad (15)$$

Just like the regular Arnoldi method, V_m transforms the matrix A into a much smaller matrix $H_m K_m^{-1} \approx V_m^\dagger A V_m$. When $\xi_k = \infty \forall k$, $K_m = \mathbb{I}_m$ and we get the regular Arnoldi relation $H_m \approx V_m^\dagger A V_m$. Of course, the greater the number of steps m , the greater is the accuracy of this approximation. For further details, we refer the reader to a comprehensive review article.³² As in our previous work,²⁵ we used the Arnoldi iteration with a Hermitian inner product instead of the complex symmetric Lanczos iteration,^{16,36} which yields Hessenberg matrices instead of complex symmetric tridiagonal matrices.

Note that we choose the shifts to be purely imaginary, i.e., $\xi = 2\pi i f$. We now show how this rational Arnoldi basis aids the computation of 2D-ELDOR spectra,

$$\begin{aligned} S_{c-}(f_1, T_{\text{mix}}, f_2) &\propto \langle z(f_2) | P_{-1 \leftarrow 0} e^{-\mathcal{L}_0 T_{\text{mix}}} P_{0 \leftarrow +1} | z(f_1) \rangle \\ &= \langle v_0 | (\mathcal{L}_{-1} + 2\pi i f_2 \mathbb{I})^{-1} P_{-1 \leftarrow 0} e^{-\mathcal{L}_0 T_{\text{mix}}} P_{0 \leftarrow +1} \\ &\quad \times (\mathcal{L}_{+1} - 2\pi i f_1)^{-1} | v_0 \rangle \\ &= e_1^\dagger \left((H_m K_m^{-1})^\dagger + 2\pi i f_2 \mathbb{I} \right)^{-1} V_m^\dagger P_{-1 \leftarrow 0} e^{-\mathcal{L}_0 T_{\text{mix}}} \\ &\quad \times P_{0 \leftarrow +1} V_m (H_m K_m^{-1} - 2\pi i f_1 \mathbb{I})^{-1} e_1. \end{aligned} \quad (16)$$

Here, e_1 is the first m -dimensional vector $e_1 = (1, 0, \dots, 0)$. We can also write $V_m e_1 = v_1$, where v_1 is the normalized starting vector, i.e., $v_1 = \frac{v_0}{\|v_0\|}$, cf. Algorithm 3. In other words, v_1 becomes e_1 under the rational Arnoldi basis. Note that $\mathcal{L}_{-1} = \mathcal{L}_{+1}$.²⁷

While evaluating 2D-ELDOR spectra using the regular Arnoldi algorithm,²⁵ we solve $(\mathcal{L}_{+1} - 2\pi i f_j \mathbb{I})^{-1} | v_0 \rangle$ for each value of f_j . Whereas in Eq. (16), we need to solve $(\mathcal{L}_{+1} - \xi_k \mathbb{I})^{-1} | v_0 \rangle$ for merely m values of ξ_k . And given the decay in the magnitude of singular values we saw in Fig. 2, we can expect m to be much smaller than n , the number of frequency grid points $\{f_1, f_2, \dots, f_n\}$. In fact, a good choice of m is just the number of significant singular values. Thus, we transform the $N \times N$ matrix A into the smaller $m \times m$ matrices H_m and K_m by means of the transformation with the $N \times m$ unitary matrix V_m from which all the required $|z(f_j)\rangle$'s, $j \in \{1, 2, \dots, n\}$, may then be readily calculated.

That is, expressions such as $(H_m K_m^{-1} - 2\pi i f_j \mathbb{I})^{-1} e_1$ are cheap to compute given the much smaller values of m compared to N . And for pulsed experiments such as 2D-ELDOR, $e^{-\mathcal{L}_0 T_{\text{mix}}} P_{0 \leftarrow +1} V_m$ is much faster to compute when compared to our original algorithm of evaluating $e^{-\mathcal{L}_0 T_{\text{mix}}} P_{0 \leftarrow +1} |z(f_j)\rangle$ for all n values of f_j .

B. Adaptive shift choice

The performance of the rational Arnoldi algorithm depends crucially on the shifts ξ_i we choose. The choice of shifts helps us to control the convergence of the algorithm. We shall adopt a *greedy heuristic*³⁵ to evaluate the next best shift ξ_{k+1} , given the shifts ξ_1, \dots, ξ_k . A greedy heuristic³⁷ builds up a solution in small steps, choosing a decision that is locally optimal at each step.

We describe here the intuition behind the process of evaluating the next shift. Given $\xi_1, \xi_2, \dots, \xi_k$, the best rational Arnoldi

approximation for a resolvent $(A - sI)^{-1} v_1$ [cf. Eq. (15)] is given as³⁵ (note that $v_1 = \frac{|v_0\rangle}{\|v_0\|}$ is the normalized starting vector, cf. Algorithm 3)

$$(A - s\mathbb{I})^{-1} v_1 \approx V_k (H_k K_k^{-1} - s\mathbb{I}_m)^{-1} V_k^\dagger v_1. \quad (17)$$

Here, \mathbb{I}_k is the $k \times k$ identity matrix. Equation (17) can be rewritten as

$$v_1 \approx (A - s\mathbb{I}) V_k (H_k K_k^{-1} - s\mathbb{I}_m)^{-1} V_k^\dagger v_1. \quad (18)$$

The error in the approximation can be described as:

$$\|v_1 - (A - s\mathbb{I}) V_k (H_k K_k^{-1} - s\mathbb{I}_m)^{-1} V_k^\dagger v_1\|. \quad (19)$$

The expression in Eq. (19) can be expressed as follows:³⁵

$$\|v_1 - (A - s\mathbb{I}) V_k (H_k K_k^{-1} - s\mathbb{I}_m)^{-1} V_k^\dagger v_1\| = \frac{|r_k(A)v_1|}{|r_k(s)|}. \quad (20)$$

Here, r_k is defined as

$$r_k(z) = \frac{\prod_{j=1}^k (z - \lambda_j)}{\prod_{j=1}^k (z - \lambda_j)}. \quad (21)$$

$\{\lambda_j\}$ are the eigenvalues of $H_k K_k^{-1}$. The term on the right-hand side of Eq. (20) dependent on s is just $\frac{1}{|r_k(s)|}$. Now, we wish to choose an s such that $(A - s\mathbb{I})^{-1}$ cannot be captured by the current rational Arnoldi approximation of order k . This implies that s should be such that $\frac{1}{|r_k(s)|}$ is maximized so that we choose the next shift to be at a location where $(A - s\mathbb{I})^{-1} v$ cannot be well-approximated by the current k th order rational Arnoldi approximation $V_k (H_k K_k^{-1} - s\mathbb{I}_k)^{-1} V_k^\dagger v_1$. This way, the new rational Arnoldi basis vector v_{k+1} will cover unexplored regions of the rational Krylov subspace in the best possible way.

Maximizing $1/|r_k(s)|$ is of course equivalent to minimizing $|r_k(s)|$. Assume that we have calculated shifts $\xi_1, \xi_2, \dots, \xi_k$. The next shift ξ_{k+1} can be evaluated as follows:

$$\xi_{k+1} = \arg \min_{s \in S} r_k(s) = \arg \min_{s \in S} \frac{|\prod_{j=1}^k (s - \lambda_j)|}{|\prod_{j=1}^k (s - \xi_j)|}. \quad (22)$$

Here, λ_j 's are the eigenvalues of $H_k K_k^{-1}$. Note that $H_k K_k^{-1}$ is a non-normal matrix just like A . Therefore, the eigenvalues are not to be trusted as accurate, as discussed in the previous work.^{16,38} Hence, we modify the greedy heuristic³⁵ slightly to avoid calculating λ_j 's by replacing the product $|\prod_{j=1}^k (s - \lambda_j)|$ with $|\det(s\mathbb{I} - H_k K_k^{-1})|$. This simplification comes from the matrix identity

$$\det(M) = \prod_{p=1}^n \lambda_p, \quad (23)$$

i.e., the determinant of a matrix M is the product of its eigenvalues. The advantage here is that we avoid the need to calculate non-normal eigenvalues and can evaluate the determinant using other methods, viz., LU decomposition, which is implemented in MATLAB's *det* function.³⁹

We now assume the set from which we choose the optimum value of s to be defined as $S \equiv [2\pi f_{min}, 2\pi f_{max}]$, where f_{min} and f_{max} denote the bandwidth of frequencies where we expect to see an ESR spectrum. At 95 GHz and motional rates $\sim 10^5 \text{ s}^{-1}$, this range could be as large as $\sim 150 \text{ G}$ or $\sim 420 \text{ MHz}$.²⁵ We adopt the following heuristic for choosing $2\pi f_{min}$ and $2\pi f_{max}$ based on our prior estimates of the range of frequencies that are significant to the 2D-ELDOR/CW spectrum at a given motional rate $R_{||}$: $2\pi f_{min} = -100 + 20(\log_{10} R_{||} - 5)$ and $2\pi f_{max} = 120 - 20(\log_{10} R_{||} - 5)$ (in Gauss units, about the center of the spectrum).

Solving for s at each step of the rational Arnoldi algorithm is a relatively inexpensive operation suitable for off-the-shelf functions such as `fminbnd` in MATLAB. Sampling based optimization techniques and modifications to the search space for the next shift in the complex might lead to a further speedup in the evaluation of successive shifts, but we chose not to pursue them. We used MATLAB's `fminbnd` function^{40,41} in this work. For rational Arnoldi iterations, we used a state-of-the-art rational Krylov toolbox⁴² written in MATLAB.

It is relevant to consider whether this heuristic gives an advantage over a simple-minded choice of shifts, such as an array of equally spaced shifts between $2\pi f_{min}$ and $2\pi f_{max}$. Figure 3 shows how the greedy heuristic leads to better convergence to the actual ESR spectrum when compared to the case where equally spaced shifts ξ_k are chosen.

While evaluating adaptively chosen shifts, we also have the option of specifying a few initial shifts before evaluating the succeeding shifts. In our work, we choose $\xi_1 = 0$, $\xi_2 = 2\pi f_{min}$, and $\xi_3 = 2\pi f_{max}$ as our three initial shifts. The remaining rational Arnoldi basis vectors and shifts ξ are calculated one by one and their corresponding rational Arnoldi vectors are added to the existing rational Arnoldi basis.

We compare the performance of the rational Arnoldi algorithm with adaptively chosen shifts, rational Arnoldi with the same

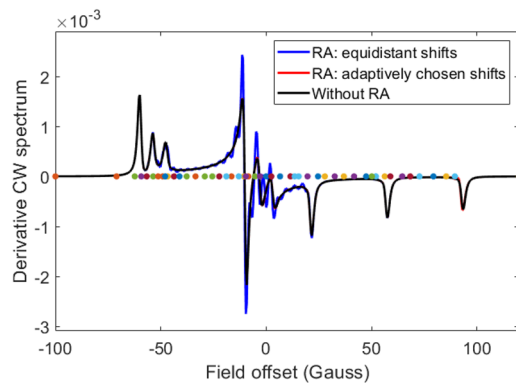


FIG. 3. Adaptive shift choices (red) outperform equally spaced shifts (blue) for a rational Arnoldi basis of size $m = 50$. The black curve corresponds to the regular Arnoldi algorithm to calculate the CW spectrum, and the red curve overlaps perfectly with it. Here, $R_{||} = 10^5 \text{ s}^{-1}$. Other parameters are as in Fig. 2. The dots on the x-axis indicate the adaptively chosen shifts used for the rational Arnoldi CW spectrum calculation with adaptively chosen shifts. The times taken for rational Arnoldi with equally spaced shifts, rational Arnoldi with adaptively chosen shifts, and regular Arnoldi were, respectively, 38 s, 53 s, and 311 s.

number but equidistant shifts, and regular Arnoldi in Fig. 3. While the rational Arnoldi algorithm with equally spaced shifts runs faster than the rational Arnoldi algorithm with adaptively chosen shifts, we must bear in mind that some of the equally spaced shifts lie in “uninteresting” frequency regions of the spectrum where the spectrum is negligible, causing faster convergence in the resolvents corresponding to such frequencies. On the other hand, adaptively chosen shifts are adept at locating the important frequency regions of the ESR spectrum and as a result, yield the more accurate results.

C. Time advantage from the rational Arnoldi approach

While evaluating resolvents at each frequency f_j takes up a significant amount of time, the real time advantage from a rational Arnoldi procedure occurs in subsequent parts of calculating a pulsed ESR experiment, viz., 2D-ELDOR. The reason is that a rational Arnoldi procedure first accurately shrinks the effective number of frequency grid points. That is, for the off-diagonal space resolvents occurring in CW and 2D-ELDOR spectra, \mathcal{L}_{+1} is N_{+1} -dimensional so that for all n resolvent calculations $(\mathcal{L}_{+1} - 2\pi f_j)^{-1}|v_0\rangle$ at the corresponding frequency points $\{f_1, f_2, \dots, f_n\}$ with regular Arnoldi, we use an N_{+1} dimensional matrix.

As shown in Fig. 4(a), in the regular Arnoldi algorithm for computing 2D-ELDOR spectra, one calculates $|z(f)\rangle = (\mathcal{L}_{+1} - 2\pi f)^{-1}|v_0\rangle$ for $f \in \{f_1, f_2, \dots, f_n\}$ and then applies the pulse propagator $P_{0 \leftarrow +1}$ to calculate $|y(f)\rangle = P_{0 \leftarrow +1}|z(f)\rangle$ with the $y(f)$ represented in an N_0 dimensional basis set in $p^S = 0$ coherence subspace and finally calculate $|x(f)\rangle = e^{-\mathcal{L}_0 T_{mix}} P_{0 \leftarrow +1}|z(f)\rangle$ for each f_i , all with the N_{+1} dimensional \mathcal{L}_{+1} matrix. To express this mathematically, we rewrite Eq. (7) as follows:

$$\begin{aligned} S_{c-}(f_1, T_{mix}, f_2) &\propto \langle v_0 | (\mathcal{L}_{-1} + 2\pi f_2 \mathbb{I})^{-1} P_{-1 \leftarrow 0} e^{-\mathcal{L}_0 T_{mix}} \\ &\quad \times P_{0 \leftarrow +1} (\mathcal{L}_{+1} - 2\pi f_1)^{-1} |v_0\rangle \\ &= \langle z(f_2) | P_{-1 \leftarrow 0} e^{-\mathcal{L}_0 T_{mix}} P_{0 \leftarrow +1} |z(f_1)\rangle \\ &= \langle y(f_2) | e^{-\mathcal{L}_0 T_{mix}} |y(f_1)\rangle \\ &= \langle y(f_2) | |x(f_1)\rangle. \end{aligned} \quad (24)$$

(Here we are implicitly using $\mathcal{L}_{-1} = \mathcal{L}_{+1}^\dagger$ and $P_{-1 \leftarrow 0} = P_{0 \leftarrow +1}^\dagger$, as detailed in the previous work.²⁷)

However, the rational Arnoldi algorithm, shown in Fig. 4(b), helps us reduce the effective number of frequencies f_1 in Eqs. (7) and (24) from $n \sim 250$ to $m \lesssim 60$. In other words, $e^{-\mathcal{L}_0 T_{mix}}$ has to act on only the m vectors, namely, the columns of $P_{0 \leftarrow +1} V_m$, rather than to act on n vectors $|y(f_i)\rangle$.

For computing the action of the diagonal space matrix exponential $e^{-\mathcal{L}_0 T_{mix}}$, we use the Expokit package¹⁸ as in our earlier work.²⁵ Note that there are other approaches for speeding up Krylov computations of the action of $e^{-\mathcal{L}_0 T_{mix}}$ than the Expokit method¹⁸ we use, such as the matrix exponential recycling method.^{43,44}

Evaluating the action of $e^{-\mathcal{L}_0 T_{mix}}$ on just the m columns of $P_{0 \leftarrow +1} V_m$ is a sufficient and compact way to determine the effect of the time evolution with respect to mixing time T_{mix} on any of the vectors propagated from the $p^S = +1$ coherence subspace. This is in contrast with the regular Arnoldi algorithm, where we have to

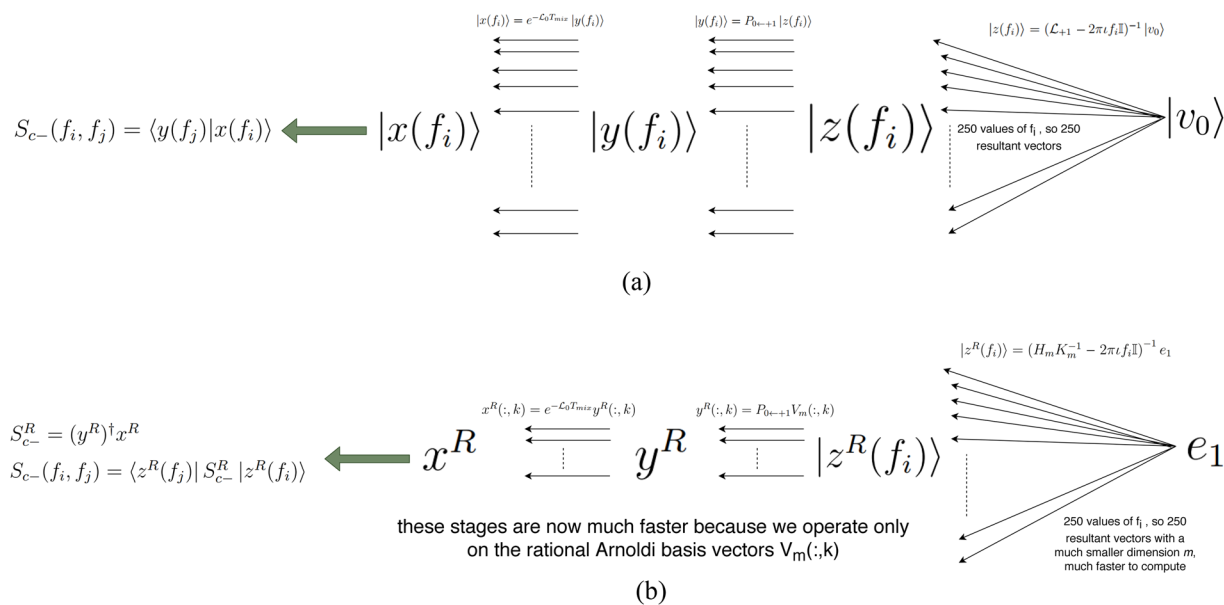


FIG. 4. Schematic describing how the rational Arnoldi algorithm speeds up 2D-ELDOR calculations at different motional rates. (a) The regular Arnoldi procedure and (b) the rational Arnoldi procedure. The superscript “R” stands for “rational Arnoldi.” The notation $A(:, k)$ indicates the k th column of matrix A .

separately evaluate the time evolution, T_{mix} , on each of the n vectors of dimension N_0 getting propagated from the $p^S = +1$ coherence subspace corresponding to a different frequency f_1 . This compression of a large ($n \sim 250$) number of vectors, each of dimension N_0 , getting propagated from the $p^S = +1$ coherence subspace is the real power of rational Arnoldi methods over regular Arnoldi methods. Finally, $|z^R(f_i)\rangle := (H_m K_m^{-1} - 2\pi i f_1 \mathbb{I})^{-1} e_1$ for $n \sim 250$ values of f_1 takes an almost negligible amount of time, as they involve $m \times m$ matrices, where $m \lesssim 60$ vs $N_{+1} \sim O(10^4)$ and $N_0 \sim 2N_{+1}$ at the ultra-slow motional rates of interest to us. To express this mathematically, we rewrite Eq. (16) as follows:

$$\begin{aligned}
 S_{c-}(f_1, T_{mix}, f_2) &\propto e_1^\dagger \left((H_m K_m^{-1})^\dagger + 2\pi i f_2 \mathbb{I} \right)^{-1} V_m^\dagger P_{-1 \leftarrow 0} \\
 &\quad \times e^{-\mathcal{L}_0 T_{mix}} P_{0 \leftarrow +1} V_m (H_m K_m^{-1} - 2\pi i f_1 \mathbb{I})^{-1} e_1 \\
 &= \langle z^R(f_2) | V_m^\dagger P_{-1 \leftarrow 0} e^{-\mathcal{L}_0 T_{mix}} P_{0 \leftarrow +1} V_m | z^R(f_1) \rangle \\
 &= \langle z^R(f_2) | (y^R)^\dagger e^{-\mathcal{L}_0 T_{mix}} y^R | z^R(f_1) \rangle \\
 &= \langle z^R(f_2) | (y^R)^\dagger x^R | z^R(f_1) \rangle \\
 &= \langle z^R(f_2) | S_{c-}^R | z^R(f_1) \rangle.
 \end{aligned} \tag{25}$$

In Eq. (25), $y^R = P_{0 \leftarrow +1} V_m$, $x^R = e^{-\mathcal{L}_0 T_{mix}} y^R$, and $S_{c-}^R = (y^R)^\dagger x^R$. y^R denotes the rational Arnoldi basis vectors transformed from $p^S = +1$ to $p^S = 0$ coherence subspace. x^R denotes the time evolution in the $p^S = 0$ coherence subspace of the transformed rational Arnoldi vectors that form the columns of y^R . S_{c-}^R is the reduced S_{c-} spectrum evaluated on the rational Arnoldi basis vectors that constitute the columns of V_m . The rational Arnoldi algorithm reduces the space

spanned by all the resolvents $|z(f)\rangle$ in the regular Arnoldi algorithm to m orthonormal vectors, namely, the columns of V_m . The columns of V_m form a *rational Arnoldi basis* for $z(f)$, $f \in \{f_1, f_2, \dots, f_n\}$. Therefore, by evaluating $S_{c-}^R = (y^R)^\dagger x^R = (y^R)^\dagger e^{-\mathcal{L}_0 T_{mix}} y^R = V_m^\dagger P_{-1 \leftarrow 0} e^{-\mathcal{L}_0 T_{mix}} P_{0 \leftarrow +1} V_m$, we have computed a minimalistic 2D-ELDOR S_{c-} spectrum and saved computation time. The minimalistic S_{c-}^R spectrum can be readily generalized to the usual S_{c-} spectrum by using $S_{c-} = \langle z^R(f_2) | S_{c-}^R | z^R(f_1) \rangle$, as in Eq. (25).

The action of $e^{-\mathcal{L}_0 T_{mix}}$ is the most time consuming part of a 2D-ELDOR calculation, given the long mixing times T_{mix} we typically have, requiring us to break the matrix exponential into multiple time steps for accuracy.³⁸ The same could be said of other multi-dimensional pulse experiments.⁴⁵

We now apply the rational Arnoldi algorithm with adaptive shifts for the following calculations: CW and 2D-ELDOR.

IV. RESULTS

A. Application to CW calculations

For motional rates $R_{||} = 10^5 \text{ s}^{-1}, 10^6 \text{ s}^{-1}, 10^7 \text{ s}^{-1}, 10^8 \text{ s}^{-1}$, we show in Fig. 5 CW spectra calculated by regular Arnoldi and the rational Arnoldi approach. For each plot, we indicate the dimension m of the rational Arnoldi approximation, along with N_{+1} , and the dimension of the SLE matrix \mathcal{L}_{+1} used for calculating the CW spectrum. These computations were performed on a Windows 10 Enterprise desktop computer with an Intel(R) Core(TM) i5-6500 CPU at 3.2 GHz processor. The respective computation times are shown in Table 1. We used the restarted Matlab GMRES solver⁴⁶ with a tolerance of 10^{-7} , which restarts after every 20 inner iterations and a maximum of 100 outer iterations. In this work, we have not

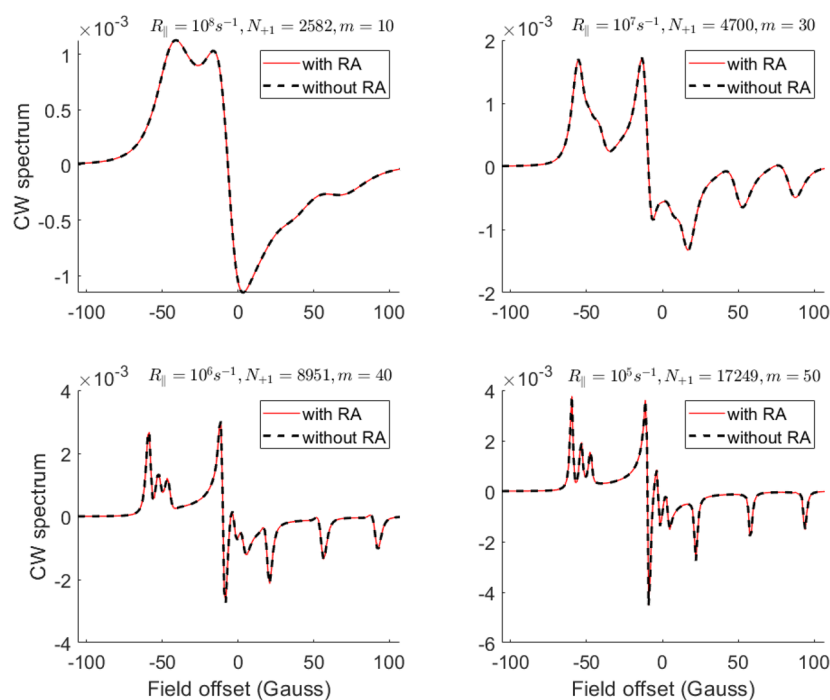


FIG. 5. CW calculations using the rational Arnoldi (RA) algorithm with adaptively chosen shifts for different motional rates: $R_{||} = 10^8 \text{ s}^{-1}$, $R_{||} = 10^7 \text{ s}^{-1}$, $R_{||} = 10^6 \text{ s}^{-1}$, and $R_{||} = 10^5 \text{ s}^{-1}$. Here, the number of shifts chosen for the regular Arnoldi algorithm (black dotted lines) is $n = 250$. The CW spectra obtained using the rational Arnoldi algorithm are shown as red continuous lines. We observe a perfect overlap between the rational Arnoldi and regular Arnoldi calculations, as expected. The respective computation times are shown in Table I. The times taken for $n = 200$ shifts are $\sim 80\%$ of the times taken for $n = 250$ shifts.

explored the tradeoffs between various combinations of tolerance, inner iterations, and outer iterations.

It is important to highlight that CW calculations via the rational Arnoldi method are mainly for illustration purposes, and one should not normally use the rational Arnoldi or regular Arnoldi method for calculations of CW spectra for the case of nitroxide spin labels. The complex symmetric Lanczos algorithm for CW spectra avoids non-normal eigenvalues and is trustworthy for slow and ultra-slow motional CW calculations^{17,27} and significantly faster than regular Arnoldi and rational Arnoldi methods. The results for CW spectra are meant to compare results for the two Arnoldi methods.

Table I presents times taken for $n = 250$ shifts for the regular Arnoldi calculation for the sake of consistency with the 2D-ELDOR calculations presented in Subsection IV B, although $n = 200$ provides sufficient accuracy for CW spectra for which the times are $\sim 80\%$ of those shown. For transition metal ions where one has to cover a much wider spectrum over many Gauss, it is

necessary to calculate the CW spectrum at each field position^{17,24} using complex symmetric conjugate gradients¹⁷ or Arnoldi methods.²⁵ In such cases, even for CW spectra, the rational Arnoldi algorithm can lead to significant time saving over the regular Arnoldi algorithm, as suggested by the results in Table I for the case of nitroxide spectra.

Another important observation, which also applies to 2D-ELDOR computations, is that the bulk of the computation time in these rational Arnoldi calculations is taken up by computing the m resolvents of the $N_{+1} \times N_{+1}$ SLE matrix \mathcal{L}_{+1} . The n computations with the rational Arnoldi algorithm are performed with much smaller, albeit dense, SLE matrices of order $m \times m$, which are much faster to calculate than the much larger, albeit sparse, $N_{+1} \times N_{+1}$ SLE matrices. We observed the resolvents of the $m \times m$ reduced matrices to be on average ~ 5000 times faster to calculate than the resolvents of the $N_{+1} \times N_{+1}$ matrices across the range of motional rates we considered in this paper.

TABLE I. Comparison of computation times for CW ESR spectra in Fig. 5.

$R_{ } (\text{s}^{-1})$	Time for regular Arnoldi with 250 shifts (s)	Time for rational Arnoldi with adaptively chosen shifts (s)	N_{+1}	m
10^8	37	3	2 582	10
10^7	57	13	4 700	30
10^6	90	24	8 951	40
10^5	165	53	17 249	50

B. Application to 2D-ELDOR calculations

We show the 2D-ELDOR spectrum with and without the rational Arnoldi algorithm in Fig. 6. Using the rational Arnoldi algorithm shows comparable accuracy at a much faster speed, as we expect. These ultra slow motional 2D-ELDOR spectra show broad motional cross-peaks^{25,27} as a function of mixing time as expected. We should reiterate that this time advantage is dependent on the motional rate. At slower motional rates, singular values decay slower, thereby requiring more rational Arnoldi iterations. By analogy with Table I for CW spectra, we expect greater time saving for the relatively faster motions.

Another point to note here is that the time improvement for the rational and regular Arnoldi algorithms scales according to

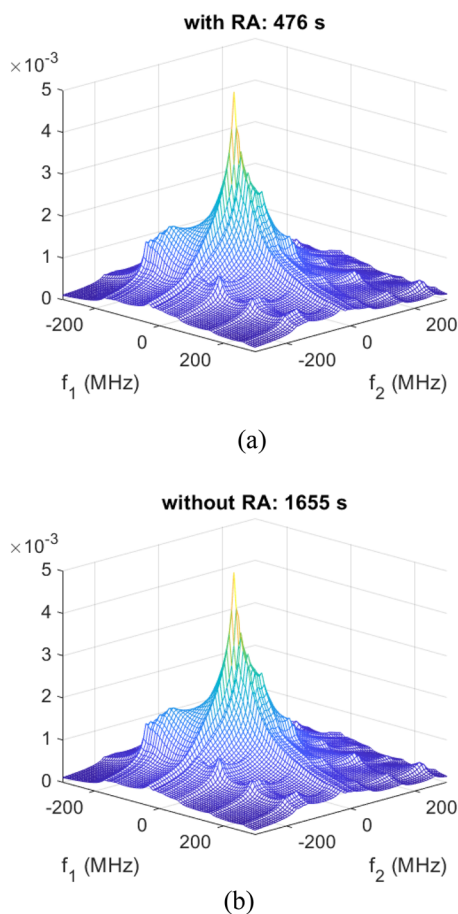


FIG. 6. Ultra-slow motional 2D-ELDOR spectra describing how the rational Arnoldi (RA) algorithm speeds up 2D-ELDOR calculations. (a) The rational Arnoldi algorithm and (b) original algorithm.²⁵ Here, $R_{\parallel} = 10^5 \text{ s}^{-1}$, $R_{\perp} = R_{\parallel}/2$, dynamic exchange rate²⁵ $k_{\text{sym}} = 10^6 \text{ s}^{-1}$, mixing time $T_{\text{mix}} = 500 \text{ ns}$, and size of Arnoldi basis $m = 60$ to ensure a sufficiently accurate 2D-ELDOR spectrum. Other parameters are same as in Fig. 5. The speedup is $\frac{1655}{476} \approx 3.5$. In the rational Arnoldi algorithm for computing 2D-ELDOR spectra in (a), 113 s out of the 476 s were spent in computing the rational Arnoldi basis and the adaptively chosen shifts. The remaining time is mostly spent in calculating the effect of the matrix exponential in the $p^S = 0$ coherence subspace, i.e., $e^{-\mathcal{L}_0 T_{\text{mix}}}$.

the desired level of resolution in the spectrum—just as the regular Arnoldi algorithm requires a smaller number of frequencies n , the rational Arnoldi algorithm requires a smaller number of shifts m for a 2D-ELDOR or CW spectrum with lower resolution.

C. Application to basis set MTS pruning

Before performing extensive calculations or non-linear least squares fits,⁴⁷ pruning the basis set to a minimal size is crucial. The MTS pruning algorithm³¹ arbitrarily selects a set of frequencies f across the CW spectrum to evaluate $|z(f)\rangle = (\mathcal{L}_{+1} - 2\pi i f \mathbb{I})^{-1}|v_0\rangle$. Actually, as shown in Fig. 5, one sweeps the magnetic field in CW ESR, but for consistency with 2D-ELDOR, we speak in terms of their frequency equivalents. The basis elements of $|z(f)\rangle$ that do not contribute significantly to the spectrum are then “pruned” out. However, when dealing with SLE matrices as big as $100\,000 \times 100\,000$, this choice of frequencies to use is an issue in order to be confident about the unimportant basis vectors to eliminate. Given our observations regarding the adaptive shift choices, we can now apply them with the rational Arnoldi algorithm to identify unimportant basis vectors with greater confidence.

We can use the adaptive shifts from Sec. III B to calculate the resolvents for an optimum set of frequencies from which the relevant basis vectors may be determined according to Ref. 31. Choosing shifts adaptively helps us in reducing the number of calls to a linear solver such as *GMRES*. This is in contrast with the earlier MTS pruning algorithm³¹ that utilizes a few, equally spaced shifts. The adaptive shift choice guides one to systematically choose appropriate frequencies for which to evaluate the resolvent. By calculating resolvents for multiple, equally spaced frequencies, it is possible that we do not explore all the relevant regions of the Krylov subspace, as illustrated in Fig. 3. Once a pruned basis set is obtained, it will significantly speed up both the regular Arnoldi method and the calculation of the minimal set of rational Arnoldi vectors of size m , as one repeats such calculations in the non-linear least squares fitting procedure.

V. COMMENTS AND CONCLUSION

In this work, we describe how rational Krylov techniques such as the rational Arnoldi algorithm result in order-of-magnitude savings in time. With this approach, we are now successful in computing accurate 2D-ELDOR spectra, while building a minimal rational Krylov subspace that better approximates matrix functions such as $f(A)b$ than the usual polynomial Krylov methods normally used. Our approach is general and can readily address multi-dimensional experiments involving more complicated pulse sequences.

We hope that our work will attract the attention of the chemical physics community toward such advanced Krylov methods that can help to quickly build up time efficient approximations to expressions such as the matrix exponential so that successive stages involved in computing multi-dimensional spectra for ESR and other techniques benefit from more compact representations. Further improvements to this work could include block bidirectional Krylov methods⁴⁸ to speed up the computation of $V_m^\dagger P_{-1 \leftarrow 0} e^{-\mathcal{L}_0 T_{\text{mix}}} P_{0 \leftarrow +1} V_m$, as shown in Eq. (16), so that the dot product between V_m and $P_{-1 \leftarrow 0} e^{-\mathcal{L}_0 T_{\text{mix}}} P_{0 \leftarrow +1} V_m$ is computed directly without explicitly constructing $e^{-\mathcal{L}_0 T_{\text{mix}}} P_{0 \leftarrow +1} V_m$, as the size of \mathcal{L}_0

could turn out to be prohibitively large. We did not consider such bidirectional Krylov methods given the additional issue of the non-normality of SLE matrices and the lack of a well-understood error analysis scheme.⁴⁹

SUPPLEMENTARY MATERIAL

The supplementary material PDF consists of details regarding how we determined the number of frequency grid points necessary (n) for calculating accurate 2D-ELDOR and CW spectra to be 250 and 200, respectively.

ACKNOWLEDGMENTS

This work was supported by the National Institute of General Medical Sciences (NIGMS) [Grant No. P41GM103521 (NIGMS/NIH)]. We also wish to acknowledge Professor David Bindel, Professor Stefan Guettel, Professor Alex Townsend, and Professor Zhaojun Bai for their advice regarding rational Krylov methods.

DATA AVAILABILITY

The data and computer programs that support the findings of this study are available from the corresponding author upon reasonable request.

REFERENCES

- 1 S. Lee, B. R. Patyal, S. Saxena, R. H. Crepeau, and J. H. Freed, *Chem. Phys. Lett.* **221**, 397 (1994).
- 2 D. Xu, R. H. Crepeau, C. K. Ober, and J. H. Freed, *J. Phys. Chem.* **100**, 15873 (1996).
- 3 V. S. S. Sastry, A. Polimeno, R. H. Crepeau, and J. H. Freed, *J. Chem. Phys.* **105**, 5753 (1996).
- 4 S. Saxena and J. H. Freed, *J. Phys. Chem. A* **101**, 7998 (1997).
- 5 A. J. Costa-Filho, Y. Shimoyama, and J. H. Freed, *Biophys. J.* **84**, 2619 (2003).
- 6 Y.-W. Chiang, A. J. Costa-Filho, and J. H. Freed, *J. Phys. Chem. B* **111**, 11260 (2007).
- 7 Y.-W. Chiang, A. J. Costa-Filho, B. Baird, and J. H. Freed, *J. Phys. Chem. B* **115**, 10462 (2011).
- 8 K. Earle, D. Budil, and J. H. Freed, *Advances in Magnetic and Optical Resonance* (Academic Press, 1996), Vol. 19, Chap. 3, p. 253.
- 9 P. P. Borbat, R. H. Crepeau, and J. H. Freed, *J. Magn. Reson.* **127**, 155 (1997).
- 10 W. Hofbauer, K. A. Earle, C. R. Dunnam, J. K. Moscicki, and J. H. Freed, *Rev. Sci. Instrum.* **75**, 1194 (2004).
- 11 K. A. Earle, B. Dzikovski, W. Hofbauer, J. K. Moscicki, and J. H. Freed, *Magn. Reson. Chem.* **43**, S256–S266 (2005).
- 12 P. A. S. Cruickshank, D. R. Bolton, D. A. Robertson, R. I. Hunter, R. J. Wylde, and G. M. Smith, *Rev. Sci. Instrum.* **80**, 103102 (2009).
- 13 J. M. Franck, S. Chandrasekaran, B. Dzikovski, C. R. Dunnam, and J. H. Freed, *J. Chem. Phys.* **142**, 212302 (2015).
- 14 C. Dunnam, B. Dzikovski, J. Franck, and J. H. Freed, “ACERT 95 GHz MKII ESR spectrometer,” in 21st International Society of Magnetic Resonance Conference, Berlin, Germany, 2019.
- 15 B. Dzikovski, V. V. Khramtsov, S. Chandrasekaran, C. Dunnam, M. Shah, and J. H. Freed, *J. Am. Chem. Soc.* **142**(51), 21368–21381 (2020).
- 16 G. Moro and J. H. Freed, *J. Chem. Phys.* **75**, 3157 (1981).
- 17 D. Schneider and J. H. Freed, *Lasers, Molecules and Methods*, edited by C. Hirschfelder and R. E. Wyatt (McGraw-Hill, 1989), Chap. 10, p. 431.
- 18 R. B. Sidje, *ACM Trans. Math. Software* **24**(1), 130 (1998).
- 19 V. Simoncini, *The Princeton Companion to Applied Mathematics*, edited by N. J. Higham *et al.* (Princeton University Press, 2015), Chap. 10, pp. 113–114.
- 20 I. Kuprov, *J. Magn. Reson.* **195**, 45 (2008).
- 21 I. Kuprov, *J. Magn. Reson.* **208**, 179 (2011).
- 22 I. Kuprov, *J. Magn. Reson.* **270**, 124 (2016).
- 23 S. Stoll and A. Schweiger, *J. Magn. Reson.* **178**(1), 42 (2006).
- 24 J. Lehner and S. Stoll, *J. Chem. Phys.* **152**, 094103 (2020).
- 25 P. Gupta, Z. Liang, and J. H. Freed, *J. Chem. Phys.* **152**, 214112 (2020).
- 26 J. H. Freed, G. V. Bruno, and C. F. Polnaszek, *J. Chem. Phys.* **75**, 3385 (1971).
- 27 S. Lee, D. E. Budil, and J. H. Freed, *J. Chem. Phys.* **101**, 5529 (1994).
- 28 S. Misra and J. H. Freed, *Multifrequency Electron Paramagnetic Resonance*, edited by S. Misra (Wiley-VCH Verlag GmbH & Co. KGaA, 2011), pp. 497–544.
- 29 T. A. Davis, *ACM Trans. Math. Software* **30**, 196 (2004).
- 30 E. Meirovitch, D. Ignier, E. Ignier, G. Moro, and J. H. Freed, *J. Phys. Chem.* **77**, 3915 (1982).
- 31 K. V. Vasavada, D. J. Schneider, and J. H. Freed, *J. Chem. Phys.* **86**(2), 647 (1987).
- 32 S. Guettel, *Surv. Appl. Math. Mech.* **36**(1), 8 (2013).
- 33 J.-M. Muller, *Elementary Functions: Algorithms and Implementation* (Birkhauser, 2016), Chap. 3, p. 59.
- 34 A. Ruhe, *J. SIAM Sci. Comput.* **19**(5), 1535 (1998).
- 35 V. Druskin and V. Simoncini, *Syst. Control Lett.* **60**, 546 (2011).
- 36 J. K. Cullum and R. A. Willoughby, *Lanczos Algorithms for Large Symmetric Eigenvalue Computations* (Birkhauser, Boston, 1985).
- 37 J. Kleinberg and E. Tardos, *Algorithm Design* (Addison-Wesley, 2005).
- 38 L. Trefethen and M. Embree, *Spectra and Pseudospectra* (Princeton University Press, 2005).
- 39 See <https://www.mathworks.com/help/matlab/ref/det.html> for Matlab documentation.
- 40 See <https://www.mathworks.com/help/matlab/ref/fminbnd.html> for Matlab documentation.
- 41 G. E. Forsythe, M. A. Malcolm, and C. B. Moler, *Computer Methods for Mathematical Computations* (Prentice-Hall, Englewood Cliffs, NJ, 1976).
- 42 M. Berljafa, S. Elsworth, and S. Guettel, <http://guettel.com/rktoolbox/guide/html/index.html>, 2020.
- 43 D. L. Goodwin and I. Kuprov, *J. Chem. Phys.* **144**, 204107 (2016).
- 44 G. J. Lord and D. Stone, *Appl. Math. Comput.* **307**, 342 (2017).
- 45 P. Borbat and J. H. Freed, *Biological Magnetic Resonance*, edited by L. J. Berliner, S. S. Eaton, and G. R. Eaton (Kluwer, 2000), Vol. 19, Chap. 9, p. 383.
- 46 See <https://www.mathworks.com/help/matlab/ref/gmres.html> for Matlab documentation.
- 47 D. E. Budil, S. Lee, S. Saxena, and J. H. Freed, *J. Magn. Reson., Ser. A* **120**, 155 (1996).
- 48 H. Guo and R. A. Renaut, *Numer. Linear Algebra Appl.* **11**, 75 (2004).
- 49 Z. Bai, private communication (2020).